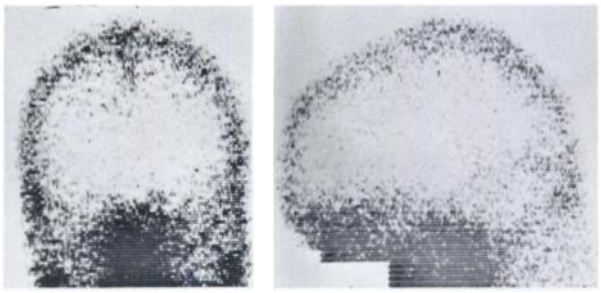

FIG. 1. Normal anterior and left lateral views performed 3 hr after injection of pertechnetate.

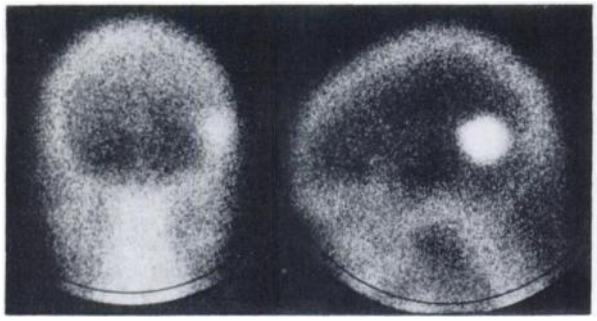

FIG. 2. Anterior and left lateral skull images made 3 hr following administration of Tc-99m diphosphonate show marked accumulation in the left parietal region.

on a rectilinear scanner with the collimator distance adjusted to bring the skull within the focal plane of the detector (Fig. 1). These were also normal. Five days later scintillation camera images of the head were performed using 20 mCi of Tc-99m diphosphonate. These showed an area of markedly increased activity in the left temporal region corresponding to the lytic skull lesion (Fig. 2). En bloc excision revealed a 3- by 3-cm, slightly raised lesion below the periosteum of the bone. The outer table was involved but the inner table and underlying dura were intact. Microscopic examination revealed typical meningioma cells with whorls and psammoma bodies. No bony elements were present.

Klein et al. recently reported a dipolic extracranial meningioma that was seen on both dynamic and static pertechnetate images (*5*). Their patient also had a corresponding lytic lesion in the parietal area on skull films. At surgery there was a large subcutaneous soft-tissue component with erosion of the outer table of the skull and extension through the inner table and dura. The large soft-tissue mass and intracranial extension may account for the better visualization in their patient with pertechnetate.

Meningiomas producing a purely lytic skull lesion are extremely rare (*6,7*). More commonly they cause an osteoblastic reaction producing a sclerotic appearance (*6*). The intraosseous location of the tumor in our patient is also unusual. Since meningiomas arise from dural elements, a possible mechanism is entrapment of dural cells along the suture line early in life. It is not known why such marked concentration of Tc-99m diphosphonate occurs in meningiomas, although it may be related in part to microscopic calcification or to increased osteoblastic activity in the surrounding bone. Accumulation within the tumor per se must also be considered since some purely intracranial tumors have been shown to concentrate Tc-99m diphosphonate. The diphosphonate may prove to be a sensitive detector of meningiomas, especially when skull involvement is present. A negative image with pertechnetate does not exclude an intraosseous meningioma.

DAVID ZARITZKY
ROBERT J. COWAN
Bowman Gray School of Medicine
North Caroline Baptist Hospital
Winston-Salem, North Carolina

REFERENCES

1. SAUER J, FIEBACH O, OTTO H, et al: Comparative studies of cerebral scintigraphy, angiography and encephalography for detection of meningiomas. *Neuroradiology* 2: 102–106, 1971

2. SHELTON J, SMOAK WM, GARGANO FP, et al.: Dynamic scintigraphy in intracranial meningiomas. *Radiology* 109: 109–115, 1973

3. GRAMES GM, JANSEN C, CARLSEN EN, et al: The abnormal bone scan in intracranial lesions. *Radiology* 115: 129–134, 1975

4. MCQUADE S, HIGGINS HP: Tc-polyphosphate in diagnosing meningiomas of the sphenoid wing. *J Nucl Med* 15: 1205–1206, 1974

5. KLEIN EW, FARHAT SM, HOSKINS PA, et al.: Radionuclide cerebral angiographic evaluation of a dipolic extracranial meningioma: Case report. *J Nucl Med* 16: 833–834, 1975

6. EVANS RW: *Histological Appearances of Tumors*, 2nd ed. Edinburgh and London, Publisher, 1966, p 393

7. HUSAINI TA: An unusual osteolytic meningioma. *J Pathol* 101: 57–58, 1970

Focal Porta-Hepatis Defect on Nuclide Imaging

The focal porta-hepatic defect on scintillation imaging has always presented a diagnostic problem. Dr. McClelland's excellent review of 40 proven cases in 1975 revealed that only 42% represented significant disease (*1*). Ten of the 40 proven cases (25%) represented malignancy. Other portal defects related to proven entities included cirrhosis, fibrosis, dilated bile ducts, viral hepatitis, hepatic laceration, cyst of the falciform ligament, and ruptured gallbladder. McClelland's review of the literature also mentioned hepatoma, abscess, infarction, choledochal cyst, and dilated splenic vein. Another 14 of his cases (35%) were considered within normal limits and other imaging modalities were not available at that time to define the defects precisely.

Recently, Sample et al. exhaustively studied 26 cases of periportal defects using a multiplane tomographic scanner as well as gray-scale ultrasound (*2*). Through precise anatomic analysis, 17 cases were proven to be normal (mostly portal venous anatomy) while five of nine (44%) were due to intrahepatic or periportal malignancies. One of Sample's abnormal cases was related to extrinsic pressure from an enlarged pancreatic carcinoma, and four other abnormlities were related to pathologically enlarged ducts.

Sample also reviewed the literature, and neither he nor McClelland note a normal kidney as causing an impression on nuclide scan that could contribute to the periportal defect. We have had two thin patients whose scans showed nonspecific periportal defects. Although intravenous urog-

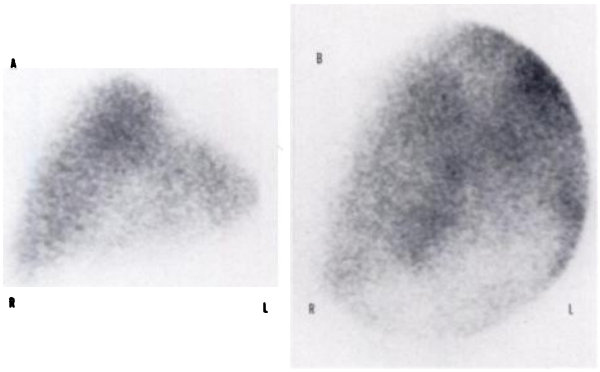

FIG. 1. (A) Anterior Tc-99m sulfur colloid scan shows portal defect. (B) Scanning after administration of DPTA shows that a normal kidney was responsible for this abnormality.

raphy noted normal renal size in these patients, renal impression was prominent on the lateral scintigram. Repeat liver imaging was then performed with DTPA, and a normal kidney was seen to be responsible for the periportal defect (Fig. 1). Long-term followup has indicated no hepatic disease. I am not implying that normal-sized kidneys contribute to the periportal defect commonly, for we have tried this technique many other times on thin patients to no avail.

The purpose of this letter is not only to add the normal kidney to the list of anatomic structures that can—although rarely—contribute to a portal defect, but also to comment on the remarkable accomplishment of Sample to remove the "nonspecific periportal defect" from nuclide reporting in his department by use of the tomographic scanner and improved ultrasound techniques.

PAUL J. MYERSON
The Griffin Hospital
Derby, Connecticut

REFERENCES

1. McCLELLAND RR: Focal porta hepatis scintiscan defects: What is their significance? *J Nucl Med* 15: 1007–1012, 1975

2. SAMPLE WF, GRAY RK, POE ND, et al: Nuclear imaging, tomographic nuclear imaging and gray-scale ultrasound in the evaluation of the porta hepatis. *Radiology* 122: 773–779, 1977

Error Due to Radionuclide Decay during Rectilinear Scanning

Short-lived radiopharmaceuticals and the gamma camera have contributed to the development of multiple diagnostic procedures in nuclear medicine. Rectilinear scanners however are still used to obtain "static images" of relatively large areas of the body. During the time required to obtain a rectilinear scan, significant radioactive decay can sometimes occur. This introduces further uncertainties into the diagnostic reliability of the image. Therefore clinical laboratories should know the magnitude of error introduced by the time interval involved in scanning. To simplify such calculations, we present a readily usable figure.

The laboratory determines two things: (a) What is the half-life of the tracer to be used? (b) What is the maximum error ("limiting error") due to decay that is acceptable during the scan (2%, 5%, 10%)?

In Fig. 1 we look up the half-life and the maximum limiting error. The vertical axis then gives the permissible scanning time so that the error due to decay is not exceeded. For example, along the horizontal axis choose 360 min (the $T_{1/2}$ of Tc-99m), and read upward to the 5% line. The corresponding vertical intercept is about 27 min. A whole-body bone scan taking longer than 27 min will have a decay factor of over 5% between beginning and end. The scanning times that do not involve 10% errors due to decay for six clinically utilized short-lived radionuclides are: Ga-68, 11 min; In-113m, 15 min; F-18, 17 min; Sr-87m, 27 min; Tc-99m, 55 min; Fe-52, 74 min.

It is possible to apply correction factors to the rectilinear scanner to compensate for the intensity losses (*1*). Below, we show the origin of the equation used to generate the above values as well as Fig. 1.

Let f be the fractional decay of the radionuclide during the scan (for example, f = 0.1 if one-tenth of the activity has decayed away). The remaining activity is then the original activity times (1 — f). In the radiodecay equation, this becomes

$$N(1 - f) = Ne^{-\lambda t},$$

or

$$1 - f = e^{-\lambda t}.$$

Solved for t (the scanning time), this equation becomes

$$t = -1.44\, T_{1/2} \ln (1 - f),$$

where ln is the logarithm to the base e and $T_{1/2}$ is the half-life of the radionuclide. This equation can be simplified by noting that for small values of f, ln (1 — f) = —f, or that $e^{-\lambda t} \approx 1 - \lambda t$ for small time intervals. The resulting equation is:

$$t = 1.44 \cdot f \cdot T_{1/2}.$$

Bear in mind that the approximation is valid only for small values of f (when elapsed times are a minor part of the half-life of the radionuclide). We also recognize that, dur-

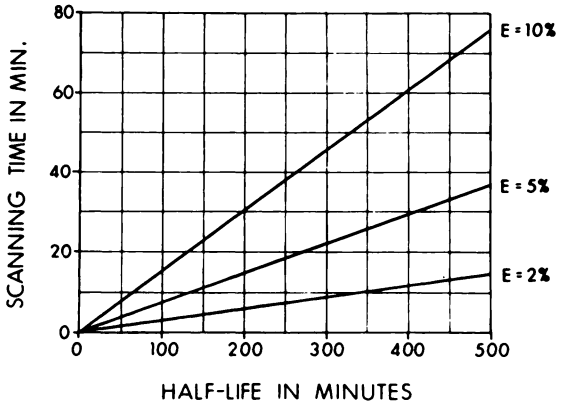

FIG. 1. Relation between half-life and scanning interval for 2, 5, and 10% limiting errors.